In-flight performance analysis of the CHAMP BlackJack GPS Receiver

Oliver Montenbruck · Remco Kroes

Abstract JPL's BlackJack receiver currently represents the most widely used geodetic grade GPS receiver for space applications. Using data from the CHAMP science mission, the in-flight performance of the BlackJack receiver has been assessed and the impact of various software updates performed during the 2.5 years since launch is described. Key aspects of the study comprise the channel allocation, anomalous data points, and the noise level of the code and carrier data. In addition, it has been demonstrated that the code measurements collected onboard the CHAMP satellite are notably affected by multipath errors in the aft-looking hemisphere, which can be attributed to cross-talk between the occultation antenna string and the primary precise orbit determination antenna. For carrier smoothed 10 s normal points, the code noise itself varies between a minimum of 5 cm at high elevations and 0.5 m (C/A) to 1.0 m (P_1, P_2) at 10° elevation. Carrier-phase data exhibit representative errors of 0.2 to 2.5 mm. The results of the CHAMP GPS data analysis contribute to a better understanding and possible improvement of the BlackJack receiver and support the design of optimal data editing and weighting strategies in precise orbit determination applications.

Keywords CHAMP · BlackJack · Multipath · Receiver noise

Received: 23 February 2003 / Revised: 31 March 2003
Accepted: 3 April 2003
Published online: 20 June 2003

O. Montenbruck (✉)
German Space Operations Center,
Deutsches Zentrum für Luft- und Raumfahrt,
82230 Weßling, Germany
E-mail: oliver.montenbruck@dlr.de
Tel.: +49-8153-281195
Fax: +49-8153-281450

R. Kroes
Delft Institute for Earth Oriented Space Research (DEOS),
Kluyverweg 1, 2926 HS Delft, The Netherlands

Introduction

Overview

This paper contains a thorough discussion and the results of an in-flight performance analysis of the CHAMP BlackJack GPS receiver. The analysis has been carried out in order to obtain a better understanding of the GPS data, and its quality, produced by JPL's BlackJack GPS receiver. Furthermore, the results can be used to develop better data editing and processing strategies as well as contribute to a better fulfillment of the CHAMP mission objectives. An introduction to both CHAMP and the BlackJack GPS receiver is given in the subsequent part of this section.

The performance analysis mainly focuses on the channel allocation process and its impact on the overall data quality, several receiver specific data errors and anomalies, the multipath problem of the BlackJack receiver and the measurement noise on both the code and carrier observations. Several new methods have been devised in order to perform the different parts of the analysis mentioned. Where appropriate, these methods are discussed in the text. The final section of this publication contains the summary and conclusions.

The CHAMP mission

The Challenging Minisatellite Payload (CHAMP) is a German small satellite mission for geoscientific and atmospheric research and applications (Reigber et al. 1996). Primary mission objectives comprise the accurate determination of the Earth's gravity field, the estimation of the magnetic field including its spatial and temporal variations, as well as the collection of refraction data for modeling the physical properties of the troposphere and ionosphere. To achieve these science goals, the satellite is equipped with a number of highly accurate instruments, such as the STAR accelerometer (ONERA, France), the BlackJack GPS receiver (JPL, USA), a laser retroreflector, a Fluxgate magnetometer, an Overhauser magnetometer, an autonomous star sensor and a digital ion driftmeter (AFRL, USA). CHAMP was launched on 15 July 2000 into an almost circular, near-polar, low-earth orbit, where it is expected to provide science data for a design lifetime of 5 years. For a more detailed description of the CHAMP mission and its scientific goals the reader is referred to Reigber et al. (1996) and CHAMP (2001).

DOI 10.1007/s10291-003-0055-5

The BlackJack GPS receiver

The BlackJack, or TRSR-2 (TurboRogue Space Receiver 2) GPS receiver, was developed by NASA's Jet Propulsion Laboratory (JPL), and is a follow-up of the TurboRogue receiver (Thomas 1995) flown earlier on missions like MicroLab-1 (GPS/MET), Oerstedt, and SunSat. In contrast to the TurboRogue receiver, which was originally built as a ground-based geodetic-grade GPS receiver, the BlackJack has been specifically designed for orbital applications. It supports a total of four antenna inputs, which can be individually assigned to any of the 48 tracking channels using a matrix switch following the amplification and digital down-conversion of the radio-frequency (r/f) signals (NASA 2001; Meehan 1997). The individual channels can be allocated in sets of three to track C/A, P_1 and P_2 code for up to 16 GPS satellites, with a typical limit of ten satellites employed on CHAMP. During Anti-Spoofing a patented, codeless tracking technique is used to estimate P-code from the encrypted Y-code (Meehan et al. 2000). Following power-up, the receiver performs a cold start search and achieves three-dimensional navigation within typically less than 15 min. Using C/A-code measurements only, the receiver position is obtained with a representative accuracy of 10–15 m in the absence of Selective Availability. In addition, the velocity of the host satellite is obtained from carrier-phase based range-rate measurements. The clock error of the receiver, obtained as part of the navigation solution, is used to steer the voltage controlled oscillator in such a way as to align the receiver time to GPS time within a tolerance margin of less than 1 μs (300 m in distance). Aside from the main tracking mode, the receiver can operate in occultation mode to collect measurements at a 50 Hz sampling rate when GPS satellites set and in altimetry mode to collect ground reflected GPS signals via a nadir-looking antenna.

The BlackJack receiver has a weight of 3.2 kg and a 15 W power consumption. While most of the electronic components are commercial-grade CMOS circuits, it has been demonstrated by total dose radiation tests that the available shielding is adequate to ensure reliable operations under space conditions (Meehan 1997). The receiver software is written as a modular, multi-threaded C++ application and is stored in flash memory. Software updates or patches can be uploaded to the spacecraft in small segments without requiring a full replacement. The available spare processor capacity can be used to implement additional non-GPS related functions as used, e.g., for star-camera processing and K-band ranging inside the GRACE receiver. Following its initial flight qualification on the Shuttle Topography mission (SIRC/X-SAR) (Bertiger et al. 2000), the TSRS-2 receiver is currently operational on the SAC-C (Meehan 1997), CHAMP, Jason-1 (Haines et al. 2002) and GRACE (Bertiger et al. 2002) satellite missions as well as the recently launched ICESat (Schutz 1998) and the Australian FedSat satellite.

CHAMP GPS antenna system

For the CHAMP mission, the receiver employs a total of four different antennas. A zenith-mounted patch antenna equipped with a choke ring and a typical cone angle of 80° serves as prime antenna for precise orbit determination (POD). A backup POD antenna and a helix antenna for occultation measurements are mounted on the rear side, which exhibits a 20° nadir tilt. Finally, a nadir-viewing helix antenna with left-hand circular polarization for GPS altimetry (using reflected GPS signals from the sea surface) is mounted on the bottom side of CHAMP. All four antennas are passive and are operated in combination with signal amplifiers inside the BlackJack receiver. While the POD antennas are commercial-grade L1/L2 patch antennas (Sensor Systems S67-1575-14) (Sensor Systems 2002), the occultation and altimetry antennas have been designed and manufactured by JPL.

Table 1
Location of the different GPS antennas on CHAMP (Lühr et al. 2001). All values are given in the spacecraft reference system and correspond to an adopted center of the antenna. The offsets of the phase centers have to be determined

Antenna	x (mm)	y (mm)	z (mm)
Main POD	−1488.0	0.0	−392.8
Reserve POD	−1738.9	0.0	−260.6
Occultation helix	−1643.1	0.0	−64.6
Altimetry helix	+857.0	241.0	233.0

The exact location of each antenna in the spacecraft reference frame can be found in Table 1 (see Lühr et al. 2001). The spacecraft reference frame originates in the center of mass and is aligned with the main body axes of CHAMP, which normally coincide with the orbital frame. The positive *z*-axis is nadir pointing (bottom), the positive *x*-axis points in along track direction (towards boom) and the positive *y*-axis (towards right) is aligned with the negative orbital angular momentum vectors thus completing a right-handed system.

Performance analysis

For the remainder of this paper, CHAMP GPS data collected by the POD antenna are used to assess the in-flight performance of the BlackJack receiver. The study extends an early flight data evaluation given in (Kuang et al. 2001) and complements laboratory based tests of the BlackJack receiver described in (Williams et al. 2002). Key issues comprise the channel allocation, outliers and data anomalies, as well as measurement noise and multipath effects that affect the distribution and quality of the obtained GPS data. Our analysis of the BlackJack receiver does not focus on a particular time period, because one of its goals is to study the improvement of the receiver and data quality over time. Over the 2.5 years that the receiver has been operational on CHAMP, several software updates were made to overcome receiver shortcomings and anomalies. Most of these updates reflect clearly in the data obtained from the receiver.

GPS observations from the primary POD antenna employed in this study have been obtained from the CHAMP Information System and Data Center (ISDC) (CHAMP

2001), which provides data starting as of May 2001. These are supplemented by the public data set for day 220/2000 (CHAMP 2000) to illustrate the behavior of the earliest BlackJack receiver software. For part of the analysis, IGS precise (final) orbits in SP3 format supplemented by 5-minute clock data have been used to model the observed pseudoranges. Precise CHAMP reference orbit were provided by DEOS (see Van den IJssel et al. 2003).

A total of nine data types are recorded in the RINEX observations files: the C/A-code (C1) and both P-code measurements (P1 and P2) as well as the carrier-phase measurements (LA, L1 and L2) and signal-to-noise ratio (SNR) for each of the associated tracking channels (SA, S1 and S2). Here, the designations in brackets have been chosen in accord with the RINEX 2.20 standard (Gurtner and Estey 2001) but differ slightly from the notation employed in the ISCD data files (L1/LP1 versus LA/L1; cf. Köhler 2001). The observations are provided at a standard data interval of 10 s and represent normal points created inside the receiver from 1 Hz samples. In the early BlackJack receiver versions, the 1 Hz pseudorange data were fit with a 10 s quadratic polynomial in order to derive the 10 s data points. This has, later on, been replaced by carrier-phase smoothing of the pseudorange data and results in a noise of the 10 s normal points that is a factor of $\sqrt{10} \approx 3$ smaller than that of the 1 s raw pseudorange data.

Throughout this paper, the code and carrier-phase observations are described by the relations:

$$\begin{aligned}
\rho_{\mathrm{CA}} &= \rho + c\Delta\delta t + b_{\mathrm{CA}} + I + M_{\mathrm{CA}} + \varepsilon_{\mathrm{CA}} \\
\rho_{\mathrm{P1}} &= \rho + c\Delta\delta t + b_{\mathrm{P1}} + I + M_{\mathrm{P1}} + \varepsilon_{\mathrm{P1}} \\
\rho_{\mathrm{P2}} &= \rho + c\Delta\delta t + b_{\mathrm{P2}} + I\tfrac{f_1^2}{f_2^2} + M_{\mathrm{P2}} + \varepsilon_{\mathrm{P2}} \\
\rho_{\mathrm{LA}} &= \rho + c\Delta\delta t - \lambda_1 N_{\mathrm{LA}} + b_{\mathrm{LA}} - I + M_{\mathrm{LA}} + \varepsilon_{\mathrm{LA}} \\
\rho_{\mathrm{L1}} &= \rho + c\Delta\delta t - \lambda_1 N_{\mathrm{L1}} + b_{\mathrm{L1}} - I + M_{\mathrm{L1}} + \varepsilon_{\mathrm{L1}} \\
\rho_{\mathrm{L2}} &= \rho + c\Delta\delta t - \lambda_2 N_{\mathrm{L2}} + b_{\mathrm{L2}} - I\tfrac{f_1^2}{f_2^2} + M_{\mathrm{L2}} + \varepsilon_{\mathrm{L2}}
\end{aligned} \tag{1}$$

in which ρ is the true geometric distance between the phase centers of the transmitting and receiving GPS antennas. The clock error difference of the GPS satellite and the BlackJack receiver is denoted by $c\Delta\delta t$ and I denotes the ionospheric path delay for the L_1 frequency (f_1). The carrier-phase ambiguities are represented by integer multiples (i.e., λN) of the respective wavelengths and b denotes additional inter-channel differences and line biases present in the receiver. Finally, the multipath and random noise are described by the M and ϵ terms, respectively.

Out of the elementary data types the common linear combinations:

$$\begin{aligned}
\rho_{\mathrm{P12}} &= \tfrac{f_1^2}{f_1^2-f_2^2}\rho_{\mathrm{P1}} - \tfrac{f_2^2}{f_1^2-f_2^2}\rho_{\mathrm{P2}} \approx 2.546\rho_{\mathrm{P1}} - 1.546\rho_{\mathrm{P2}} \\
\rho_{\mathrm{L12}} &= \tfrac{f_1^2}{f_1^2-f_2^2}\rho_{\mathrm{L1}} - \tfrac{f_2^2}{f_1^2-f_2^2}\rho_{\mathrm{L2}} \approx 2.546\rho_{\mathrm{L1}} - 1.546\rho_{\mathrm{L2}}
\end{aligned} \tag{2}$$

(Hofmann-Wellenhof et al. 1997) are formed to obtain ionosphere-free range measurements (with a roughly 3 times larger noise level than the respective single-frequency measurements) for point positioning and orbit determination. Furthermore, the Melbourne-Wübbena combination:

$$\rho_{\mathrm{MW}} = \frac{1}{f_1 - f_2}(f_1\rho_{\mathrm{L1}} - f_2\rho_{\mathrm{L2}}) - \frac{1}{f_1 + f_2}(f_1\rho_{\mathrm{P1}} + f_2\rho_{\mathrm{P2}}) \tag{3}$$

(Melbourne 1985; Wübbena 1985) is used for data screening and editing. This linear combination of narrow-lane P-code pseudoranges and wide-lane carrier-phase measurements results in a geometry-, ionosphere- and troposphere-free observable. It is less sensitive to code noise than a simple difference of ionosphere-free pseudorange and carrier measurements (cf. Eq. 2) and well suited for cycle slip and outlier detection.

Channel allocation

The number of available channels for tracking satellites and the strategy used for channel allocation have a notable influence on the quality and usefulness of the data produced by a GPS receiver. To ensure a maximum number of good quality observations with a good geometric distribution, which is relevant for both the on-board and post-processed navigation solution, the channel allocation algorithm has to select satellites based on criteria as the elevation angle and the PDOP (Position Dilution Of Precision) value. The exact channel allocation strategy used by the receiver cannot be determined from the data produced by it. However, it is possible to say something about its effectiveness, the way improvements were made to it and the resulting data quality. In order to achieve this for the BlackJack GPS receiver on CHAMP, data from multiple time periods have been used to incorporate the different software updates relevant for channel allocation issues. Two software updates made so far were identified to be relevant for the receiver channel allocation process. The first update, completed on 26 July 2001 (Meehan 2001), incorporated a change in the cut-off elevation angle of the receiver. The second update, made on 5 March 2002 (Grunwaldt, personal communication), enlarged the number of channels used for tracking. The impact of these two software updates on the receiver tracking performance and data quality is discussed with the aid of Fig. 1. It shows sky-plots and histograms for selected days before, between and after both software updates.

The sky-plots represent the direction of the line-of-sight vector from the receiver to the GPS satellite with respect to the local orbital frame that is nominally aligned with the main body axes. Its azimuth (A) is measured from the $+x$-axis (forward, A=0°) to the $+y$-axis (right, A=+90°) and the elevation angle E is measured positive towards the zenith ($-z$-direction). The histograms provide the distribution of the number of tracked and useful GPS satellites per epoch together with the total number of epochs for the given days. The number of useful satellites per epoch is derived from editing based on the elevation angle (affecting data noise and multipath), the SNR values (affecting data noise), the PDOP value (affecting single-point positioning accuracies) and the Melbourne-Wübbena combination (indicating outliers and cycle slips).

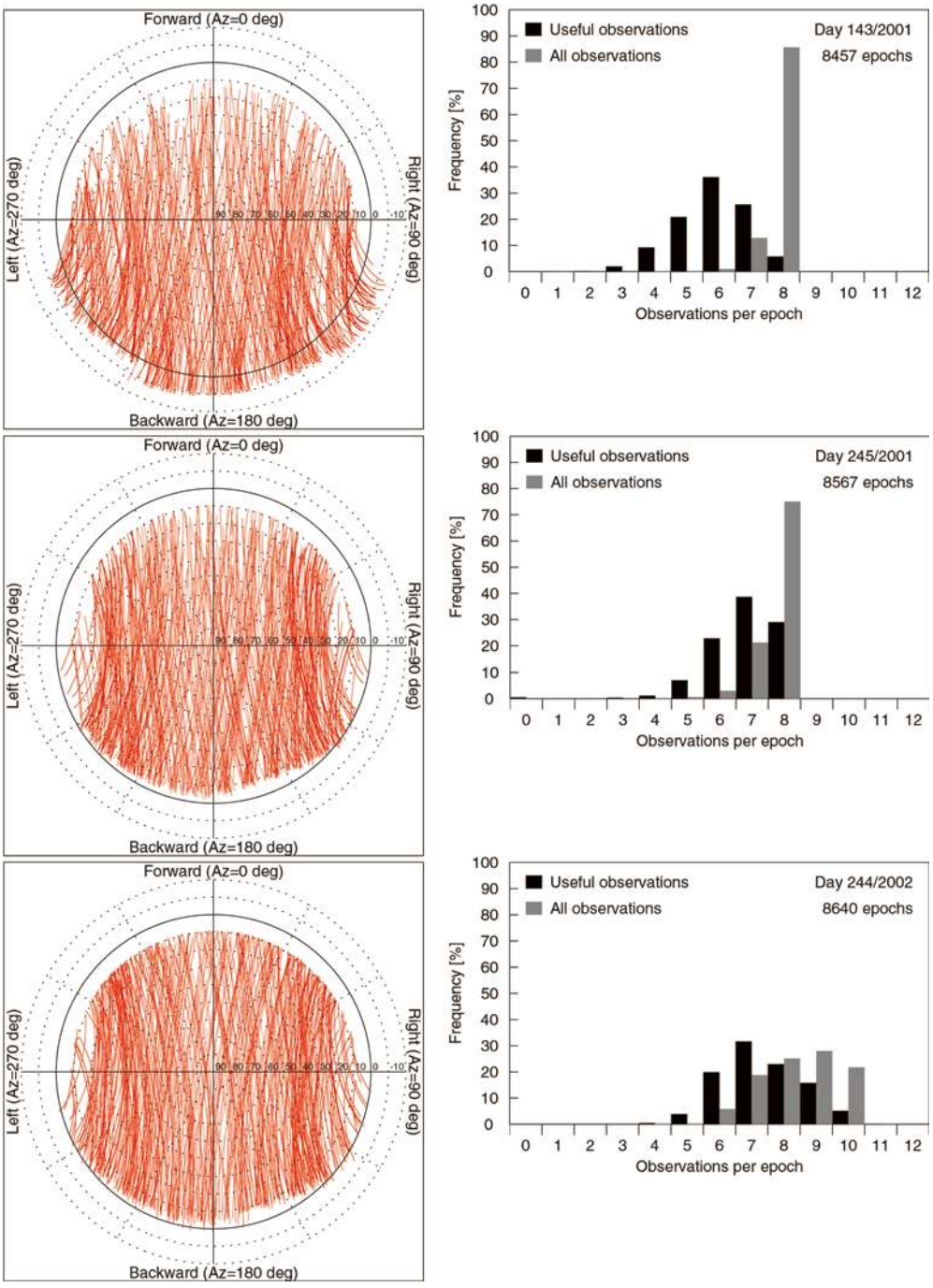

Fig. 1
Sky plots illustrating changes in the channel allocation for days 143/2001 (*top* pronounced forward/backwards asymmetry and large number of negative elevation observations), 245/2001 (*center* symmetric distribution of tracked satellites), and 244/2002 (*bottom* maximum number of tracked satellites increased from eight to ten). The associated histograms show the statistical distribution of the number of tracked satellites per epoch (*shaded*) and the distribution of the number of good observations per epoch (*black*). See text for further explanation

The different histograms immediately show that there are only eight channels active until the second software update (Fig. 1, top and center); this is then changed to ten (Fig. 1, bottom). The increase in the total number of available epochs (8,457 on day 143/2001, 8,567 on day 245/2001, 8,640 on day 244/2002) over the different time periods shows that the number of data gaps is decreasing over time. This is also visible in the different sky-plots where the data density increases per time period. The sky plots also show that the BlackJack applies an elevation threshold of approximately 10° for satellite acquisition. This feature has remained constant over time. Before the first software update, the receiver tracked satellites far below 0° elevation, at the cost of higher elevation satellites also visible at the same time. The strategy here was clearly to maintain track of a satellite as long as possible. However, the low elevation satellites deliver observations of a poorer quality (due to the decreased antenna gain and signal-to-noise ratio) resulting in less useful data for navigation for this time period. The first software update fixes this problem. The receiver now only tracks negative elevation satellites, sporadically, and acquires new satellites at a much earlier stage. As a result, a significant improvement of the overall amount of good quality data is obtained. This is supported by the change in distribution of the number of useful observations per epoch, which

changes from an average of six to an average of seven. The second update does not change this average value, but enables up to ten useful observations per epoch.

Outliers and anomalies

This section provides a discussion of outliers and anomalies encountered in the CHAMP GPS flight data. It complements and extends a previous report of BlackJack specific data anomalies encountered during signal simulators testing of the ICEsat spare receiver (Williams et al. 2002).

General outliers

At the 10 s sampling rate, the CHAMP BlackJack receiver provides a representative number of 60,000 (eight channels active) to 75,000 (ten channels active) pseudorange measurements per day. Out of these data, a small fraction exhibits errors far above the 3 σ measurement noise. To identify such outliers, we employed a kinematic point positioning method involving an iterative post-fit residuals check and data rejection. In total, about 4% outliers with errors between 10 and 100 m (in P_{12}) and 0.2% outliers with errors of 100 m and up were encountered in early 2001. Following a revision of the channel allocation, these numbers later dropped to 1 and 0.1%, respectively. This improvement can mainly be attributed to a decreased fraction of low elevation observations (E<0–10°; cf. Fig. 1) with unfavorable signal-to-noise ratios (S1, S2<15–25°). In various cases (few measurements per day), we observed erratic pseudoranges with residuals of tens to hundreds of kilometers even at high elevations. These may generally be identified and rejected based on simple integrity checks (e.g., variation of Melbourne-Wübbena combination between epochs).

Along with the analysis of code observations in the kinematic point positioning, we identified carrier-phase outliers from the post-fit residuals of differential single point solutions. Carrier-phase outliers were found to affect roughly 1% of the total number of observations from mid 2001 onwards. They are typically confined to errors of less than 1 m and can be attributed to integer cycle slips in the L1 and L2 measurements. Again, the erroneous observations are mostly confined to low elevations or SNR values and the fraction of affected measurements amounts to less than 0.1% when excluding elevations below 10°. Following the March 2002 software update, an increased amount of carrier-phase outliers (3% total, 0.5% above 10°) may be observed, which correlates with the increased carrier noise level. Among the coarse outliers, both erratic points and systematic outliers associated with erroneous locks may be observed. Aside from SNR and elevation-based edit criteria, a large fraction of the anomalous carrier measurements can well be recognized from discontinuities in the Melbourne-Wübbena linear combination.

Code biases

The BlackJack GPS receiver occasionally suffers from 15 m code biases for all or most of a pass (i.e., start of track to end of track). When occurring, all three code observations (i.e., C/A, P_1, and P_2) as well as the ionosphere-free P_{12} linear combination experience a common offset of about

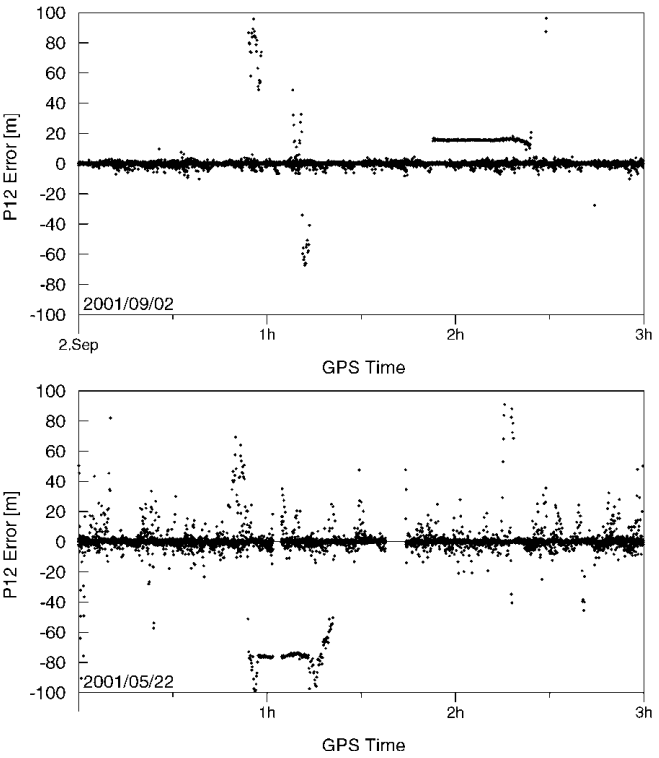

Fig. 2
Pseudorange errors (ionosphere-free P_{12} combination) for selected data arcs on day 245/2001 (*top*) and 142/2001 (*bottom*). Aside from scattered outliers, the occurrence of systematic 15 and 75 m code offsets may be recognized

15 m (Fig. 2). Based on its magnitude, this bias has previously been interpreted as half a P-code chip in (Williams et al. 2002). On average, two out of roughly 400 daily passes are affected by a 15 m bias. While the erroneous data may readily be recognized and rejected in a ground-based processing, they are difficult to discern from ephemeris and ionospheric errors inside the receiver and therefore affect the built-in C/A-code based navigation solution.

To determine the exact size of the code offset and to enable a possible correction for it, the residuals of the ionosphere-free code observations have been obtained and averaged over a single pass. The analysis has been conducted for days 140–150/2001 (i.e., the data employed in the IGS low Earth orbit campaign) and days 240–250 of 2001. Here, the anomaly occurred for a maximum of three passes per day, but some days remained unaffected. Results for a representative selection of passes can be found in Table 2. On average, the code bias amounts to 15.5±0.2 m, which is barely consistent with a half a P-code chip length and suggests an alternative interpretation. In fact, the pseudorange offsets can best be attributed to a receiver internal sampling error yielding a bias of $c{\cdot}\tau$=15.511 m at the effective sampling rate of $1/\tau=19.328{\cdot}10^6$ Hz employed in the CHAMP BlackJack receiver (Young, personal communication). Since the sampling error yields a constant offset but does not affect the measurement noise and

Table 2
Selected passes with systematic biases in ionosphere-free pseudoranges encountered during days 140–150/2001

Day	Pass (UTC)	PRN	Bias (m)
140	20:49	7	−15.56
140	16:52	24	−15.42
146	08:42	1	−15.33
146	06:34	5	+15.56
147	12:03	27	−15.62
148	20:59	28	+15.23
149	21:31	14	−15.18
149	00:05	31	+15.52
150	15:01	20	+15.73
142	00:48	10	−75.30
147	02:33	2	−74.91

signal-to-noise ratio, its predicted value of 15.511 m can be used to correct affected measurements if desired.
For completeness, we note that a sampling rate of $1/\tau$=20.456 MHz is employed in some previous models of the BlackJack receiver. Here, the size of one sample corresponds to a pseudorange error 14.65 m, which perfectly matches the value of 14.7±0.3 m (Williams, personal communication) obtained in the analysis of the ICEsat flight spare (cf. Williams et al. 2002).
Table 2 also illustrates the occasional occurrence of passes with an approximate bias of 75 m in the ionosphere-free P_{12} pseudorange combination (Fig. 2). In both of the two cases encountered during days 140–150/2001 the bias coincides with very low SNR values on the L2 frequency, which suggests a different cause than the sampling error described above. Inspection of the individual code measurements indicates that the P_2 measurement exhibits a systematic error of about 48 m at the affected epochs, while the C/A and P_1 pseudoranges appear to be error free. Other than the sampling error discussed above, the 48 m biases in the P_2 pseudoranges cannot adequately be corrected in a post-processing due to a high noise level and the lack of a model explaining the nature and exact size of this bias.

L2 ramps

The term 'L2 ramp' introduced in Williams et al. (2002) denotes a data anomaly during which the L2 carrier-phase observation exhibits a rate error of mostly ±6 m/s. L2 ramps usually start at the beginning of a satellite pass when the received signals are still weak and exhibit S2 signal-to-noise ratios that are significantly lower than the corresponding S1 value. The anomaly can easily be visualized by forming the time derivative $d(\rho_{L2}-\rho_{L1})/dt$ of the L_2–L_1 phase difference, which is nominally zero except for a small variation of the ionospheric phase advance. For automated data editing, the anomalous data can safely be identified based on the rate of change of the Melbourne-Wübbena combination.
The occurrence of L2 ramps can be attributed (Young, personal communication) to a false L_2 carrier lock with a frequency offset of 25 Hz, i.e., one-half of the navigation bit rate. At the L_2 wavelength of λ=24.4 cm, this yields an expected range rate offset of 6.1 m/s in good accord with the observations. However, due to the irregular nature of the L2 ramps, it is not feasible to correct the resulting error of the L2 observable.
In an analysis of selected data arcs collected in 2001 and early 2002 the L2 ramp anomaly was encountered multiple times per day on an almost daily basis. Other than described in (Williams et al. 2002), the P_2 code measurements were generally found to be valid during the L2 ramps. After the software update of 5 March 2002, the L2 ramps completely disappear as the result of a new consistency check between pseudorange and carrier-phase measurements that was added to the receiver software (Young, personal communication).

Sudden SNR drops and low SNR curves

During signal simulator testing of the BlackJack spare receiver for the ICEsat mission (see Williams et al. 2002) numerous outages were encountered near the center of a tracking pass, when the elevation and line-of-sight acceleration attained peak values. This anomaly is characterized by sudden SNR drops and invalid or missing pseudorange measurements from the C/A, P_1 and P_2 tracking channels. In the CHAMP BlackJack flight data, a similar problem shows up in the data set for day 220/2000, but no further indications were found in any of the examined data sets since the start of the CHAMP ISDC in May 2001. Other occurrences of anomalous SNR values may still be noted, however, during which either S1 or S2 stays low for an entire pass or a large part thereof. As noted above, the occurrence of 48 m P_2 code offsets appears to coincide with low S2 signal-to-noise ratios but no such correlation could be established for low S1 values.

Multipath errors

Multipath errors in a GPS receiver are caused by the superposition of the direct signal with interfering signals taking a different signal path. They are typically associated with signal reflections in the vicinity of the receiving antenna, in which case the resulting errors depend on the path difference, the strength and polarization of the reflected radiation as well as receiver internal properties. While carrier-phase multipath is confined to a quarter wavelength, code multipath may be as large as 0.5 code chips for distant reflectors (Leva et al. 1996; Braasch 1995). In case of a spaceborne GPS receiver, multipath reflections are exclusively caused by the satellite's surfaces (if we exclude rendezvous and docking type of applications) and the maximum path delay is thus of the order of the linear spacecraft dimension.
Evidence for code multipath errors is already contained in early analyses (Kuang 2001) of the CHAMP GPS data quality but has been widely ignored so far. It shows up in a worse-than-expected scatter of geometry- and ionosphere-free linear combinations as well as pseudorange residuals that are inconsistent with the receiver performance in a lab environment. In the context of the present work, multipath errors were first noted from a systematic bias of single point positioning results using

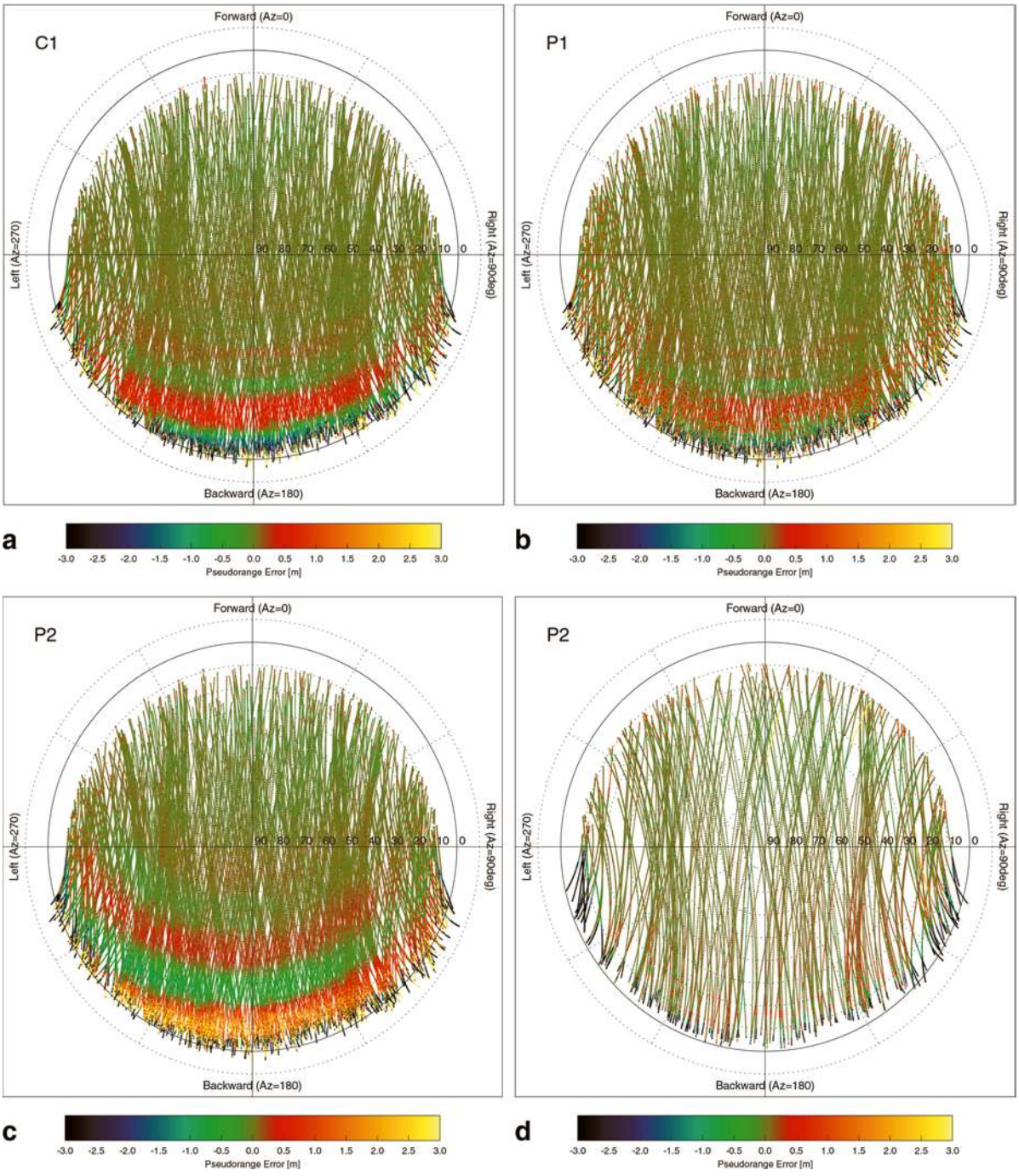

Fig. 3
a Sky plots of CHAMP multipath errors on C/A-code for days 140–141/2001. **b** Sky plots of CHAMP multipath errors on P_1-code for days 140–141/2001. **c** Sky plots of CHAMP multipath errors on P_2-code for days 140–141/2001. **d** Sky plots of CHAMP multipath errors on P_2-code during deactivation of the occultation antenna string on day 310/2002

dual frequency P-code measurements as compared to carrier based or dynamically constrained orbit determination solutions. This bias affects the radial position component by roughly −0.4 m (when considering observations down to the 0° elevation) while the along-track and cross-track position are essentially unaffected.

For further analysis of code multipath effects on CHAMP, the respective errors were isolated by forming the linear combinations:

$$\begin{aligned}
\rho_{\mathrm{CA}} - \tfrac{2}{f_1^2-f_2^2}\left(f_1^2\rho_{\mathrm{L2}} - f_2^2\rho_{\mathrm{L1}}\right) - \rho_{\mathrm{L1}} - B_{\mathrm{CA}} &\approx M_{\mathrm{CA}} + \varepsilon_{\mathrm{CA}} \\
\rho_{\mathrm{P1}} - \tfrac{2}{f_1^2-f_2^2}\left(f_1^2\rho_{\mathrm{L2}} - f_2^2\rho_{\mathrm{L1}}\right) - \rho_{\mathrm{L1}} - B_{\mathrm{P1}} &\approx M_{\mathrm{P1}} + \varepsilon_{\mathrm{P1}} \\
\rho_{\mathrm{P2}} - \tfrac{2}{f_1^2-f_2^2}\left(f_1^2\rho_{\mathrm{L2}} - f_2^2\rho_{\mathrm{L1}}\right) - \rho_{\mathrm{L2}} - B_{\mathrm{P2}} &\approx M_{\mathrm{P2}} + \varepsilon_{\mathrm{P2}}
\end{aligned} \tag{4}$$

in which the receiver-to-satellite geometry and the ionospheric errors have both been eliminated. Carrier ambiguities and differential code biases are combined in float

bias parameters $B_{C/A}$, B_{P1} and B_{P2} which are constants throughout each pass of uninterrupted carrier-phase tracking. Assuming that carrier-phase multipath and noise are much smaller than the respective code errors, the above linear combinations thus provide a direct measurement of the C/A and P1/P2 code multipath errors and noise.

Since the bias parameters B_i are not known a priori, they have to be adjusted on a per-pass basis to achieve a zero-mean right-hand side of (Eq. 4) using observations that may be considered to be free of systematic errors. In case of measurements collected with the CHAMP Precise Orbit Determination (POD) antenna one may observe that the ionosphere-free code and carrier combinations exhibit an essentially constant offset during the ascent of a GPS satellite but start to be inconsistent prior to its setting. We have therefore chosen to adjust the biases using any observations with adequate signal-to-noise ratio in the forward hemisphere but include aft looking observations only above an elevation threshold of 50°.

Sample calibrations for the multipath errors of C/A- and P-code measurements collected with the prime POD antenna of CHAMP on days 140–141 of 2001 are shown in Fig. 3a–c. Similar results are obtained for other data arcs and no indications of time varying effects have been encountered in our study. Overall, the multipath effects are confined to the aft-looking hemisphere and are most pronounced close to the satellite horizon. However, weak traces of multipath errors may even be discerned close to the zenith. For C/A-code measurements extreme multipath values of –2.0 m and +0.7 m can be observed and an almost identical distribution pattern, but roughly 60% smaller amplitude is obtained for the P_1-code measurements. The P_2 multipath effects, in contrast, vary between peak values of –0.6 m and +1.8 m and exhibit a notably shifted pattern with wider fringes.

As illustrated by the sky-plots (Fig. 3a–c), the multipath errors in the aft-looking hemisphere depend predominantly on elevation and vary only gradually with azimuth. The distribution of errors is not, however, strictly symmetric around the zenith, but exhibits an apparent pole that is mostly tilted in the forward direction and slightly offset to the left. Upon testing various combinations, we found that a coordinate system (X,Y,Z) resulting from the orbital and nominal body frame (x,y,z) by a roll rotation angle of $\Delta\vartheta \approx -7^\circ$ and a pitch rotation angle of $\Delta\psi \approx -27^\circ$ provides an almost complete decoupling of the multipath dependence on azimuth and elevation angles.

For a given unit vector $\boldsymbol{e}$ from the antenna to the observed GPS satellite, the relations:

$$\begin{pmatrix} +\cos(\varepsilon)\cos(\alpha) \\ +\cos(\varepsilon)\sin(\alpha) \\ -\sin(\varepsilon) \end{pmatrix} = \begin{pmatrix} \mathbf{e}_X^T\mathbf{e} \\ \mathbf{e}_Y^T\mathbf{e} \\ \mathbf{e}_Z^T\mathbf{e} \end{pmatrix} = \mathbf{R}_2(\Delta\psi)\mathbf{R}_1(\Delta\vartheta)\begin{pmatrix} \mathbf{e}_x^T\mathbf{e} \\ \mathbf{e}_y^T\mathbf{e} \\ \mathbf{e}_z^T\mathbf{e} \end{pmatrix} \tag{5}$$

provide the elevation ϵ above the tilted XY-plane (Fig. 4) as well as the in-plane angle α, (measured positive from the X-axis to the Y-axis). Here, $\boldsymbol{e}_X$, $\boldsymbol{e}_Y$ and $\boldsymbol{e}_Z$ denote unit

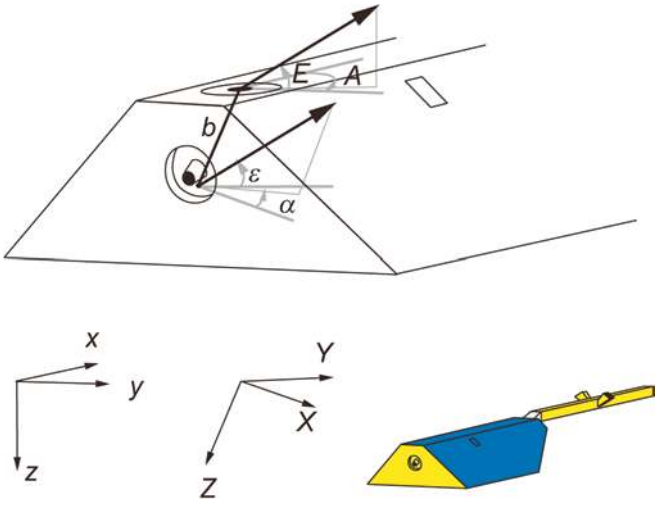

Fig. 4
CHAMP spacecraft coordinate system (x, y, z) and reference frame for multipath analysis (X, Y, Z)

vectors along the X-,Y- and Z-axes of the titled frame, while the unit vectors $\boldsymbol{e}_x$, $\boldsymbol{e}_y$ and $\boldsymbol{e}_z$ describe the main body axes. These can be identified with the along-track, cross-track, and nadir direction vectors:

$$\mathbf{e}_x = \mathbf{e}_y \times \mathbf{e}_z \quad \mathbf{e}_y = -\frac{\mathbf{r}\times\mathbf{v}}{|\mathbf{r}\times\mathbf{v}|} \quad \mathbf{e}_z = -\frac{\mathbf{r}}{|\mathbf{r}|} \tag{6}$$

as defined by the spacecraft position $\boldsymbol{r}$ and inertial velocity $\boldsymbol{v}$ during regular science mode operations.

When referred to the tilted (X,Y,Z) frame, the multipath errors exhibit a fully symmetric distribution and depend only on the elevation angle ϵ, except for a general decrease in amplitude for azimuth angles far off from 180°. Together, these observations suggest that the source of interfering radiation causing the multipath effects is located somewhere along the positive Z-axis relative to the POD antenna. Denoting the mutual distance by b, the secondary signal experiences an elevation dependent path difference d with respect to the direct signal, which, in its most general form, is described by the relation:

$$d = d_0 - b\mathbf{e}_Z^T\mathbf{e} = d_0 + b\ \sin(\varepsilon) \tag{7}$$

(Fig. 5). Here, the constant d_0 describes the delay at zero elevation, which equals the baseline in case of a reflected signal. On the other hand, Eq. (7) is likewise applicable for multipath effects caused by a secondary antenna, in which case d_0 accounts for any line or cable length differences on the way to the receiver (Fig. 5).

Following Young (1988), the code multipath error can be described by:

$$M = d\frac{m\cos(2\pi d/\lambda + \Delta\phi)}{1 + m\cos(2\pi d/\lambda + \Delta\phi)} \overset{m\ll 1}{\approx} md\cos(2\pi d/\lambda + \Delta\phi) \tag{8}$$

for multipath delays less than the 15.5 m correlator spacing. Here m is the amplitude ratio of the interfering and direct signal and λ is the L_1 wavelength (0.1905 m; for C/A- and P_1-code) or L_2 wavelength (0.2445 m; for P_2

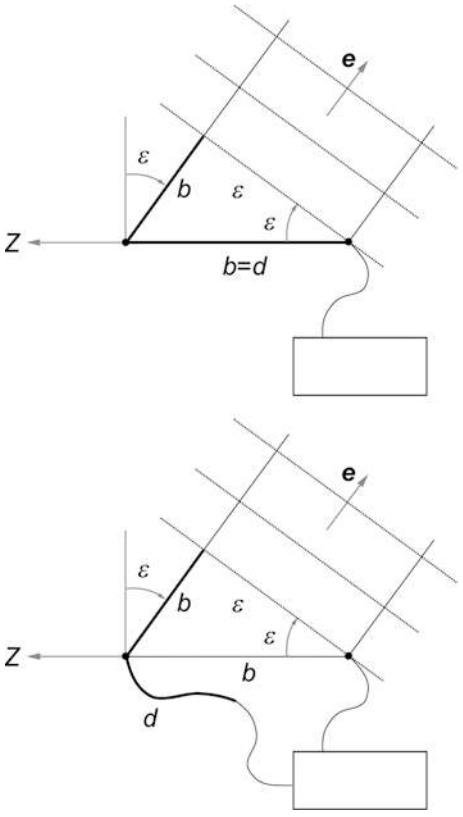

Fig. 5
Path difference for different forms of interfering radiation mixed with the prime POD antenna signal

measurements). Furthermore, $\Delta\Phi$ denotes a supplementary phase shift that may either occur upon signal reflection or in the antenna/receiver electronics.
Assuming that $m(\alpha,\epsilon)$ varies smoothly and is non-zero throughout the aft-looking hemisphere, the zones of vanishing multipath may uniquely be associated with the roots of the cosine function in (Eq. 8). For a given azimuth α, neighboring roots of $M(\epsilon)$ correspond to changes of $\Delta d = \lambda/2$ or, equivalently, $b\Delta\sin(\varepsilon) = \lambda/2$. This fact may be used to infer the length of the baseline b from the observed multipath pattern.
In order to separate multipath effects from measurement noise, the results of Eq. (4) have been averaged over intervals of ±0.5° in ϵ . Furthermore, the data set has been confined to observations within an azimuth range of α=180°±10° that exhibits the strongest multipath-to-noise ratio (Fig. 6). For observations on the L_1 frequency (i.e., C/A- and P_1-code), two consecutive nodes near elevations of ϵ=−14° and ϵ=+2° can be distinguished, which yields a baseline of:

$$b_{L1} = (\lambda_{L1}/2)/(\sin(+2^\circ) - \sin(-14^\circ)) = 0.34\text{m} \qquad (9)$$

with an expected uncertainty of about ±0.05 m. As a consequence, the interfering radiation is found to originate from a location near the occultation helix antenna, which is mounted on the aft panel of the CHAMP spacecraft with a 20° inclination towards nadir (Lühr et al. 2001, CHAMP 2001). For the P_2-code, a somewhat larger value of:

$$b_{L2} = (\lambda_{L2}/2)/(\sin(+8^\circ) - \sin(-7.5^\circ)) = 0.45\text{m} \qquad (10)$$

is obtained, which is only marginally compatible with the L_1 result, but likewise falls into the vicinity of the occultation helix. Both results therefore suggest interfering signals from the occultation antenna, rather than a reflection, as the most likely source of the observed multipath effects. This was substantiated by laboratory tests made at JPL using the CHAMP engineering model (Meehan, personal communication).
In view of remaining uncertainties caused by the inconsistent baselines and the non-zero roll angle of the empirically determined Z-axis, a test was conducted on day 310 (Nov. 6) of 2002 in which the preamplifier and front-end connected to the occultation antenna were temporarily deactivated (Grunwaldt, personal communication). As may be recognized from Fig. 3d, multipath errors do not show up during this time frame, which provides final evidence for attributing the observed errors to cross-talk between the POD and occultation antenna strings within the BlackJack receiver.
Since deactivation of the BlackJack occultation antenna string is not feasible during regular science operation, an effort has been made to derive a semi-empirical correction model for the code measurements collected with the CHAMP POD antenna. To this end, the variation of the multipath error with azimuth α and elevation ϵ is described by the expression:

$$M(\alpha,\varepsilon) = M_0\cos(\alpha-\alpha_0)\cdot 10^{-(\varepsilon-\varepsilon_0)/\Delta\varepsilon_{10}} \cdot\cos\left(\frac{2\pi}{\lambda}(d_0 + b\sin\varepsilon)\right) \qquad (11)$$

It denotes the product of a periodic term accounting for the elevation dependent path delay, an exponential term modeling the changing ratio of direct and secondary signal strength with elevation and a cosine term modeling the azimuth dependence of the signal strength ratio. The above relation is applied for all observations in the aft-looking hemisphere (defined by $\cos(\alpha\text{-}\alpha_0)>0$), otherwise the modeled multipath error is set to zero.
A set of suitable model coefficients adjusted from the individual multipath measurements is summarized in Table 3. The model provides an overall accuracy of better than 0.3 m for all observations above an elevation threshold of E=5° (cf. Fig. 7). When used in dual frequency single point positioning solutions, the empirical multipath correction was found to remove most of the radial bias observed otherwise and to reduce the overall 3D r.m.s. position error by roughly 0.6 m (ca. 20%). Even though corrections of individual ionosphere-free pseudorange may be as large as 4 m (Fig. 7), the overall improvement of the navigation solution is generally much smaller and depends notably on the applied elevation mask as well as other editing criteria.
Concerning a physical interpretation of the semi-empirical multipath model, we note that no attempt has been made to constrain the baseline length b and the 10 dB scale height $\Delta\epsilon_{10}$ to common values for the different

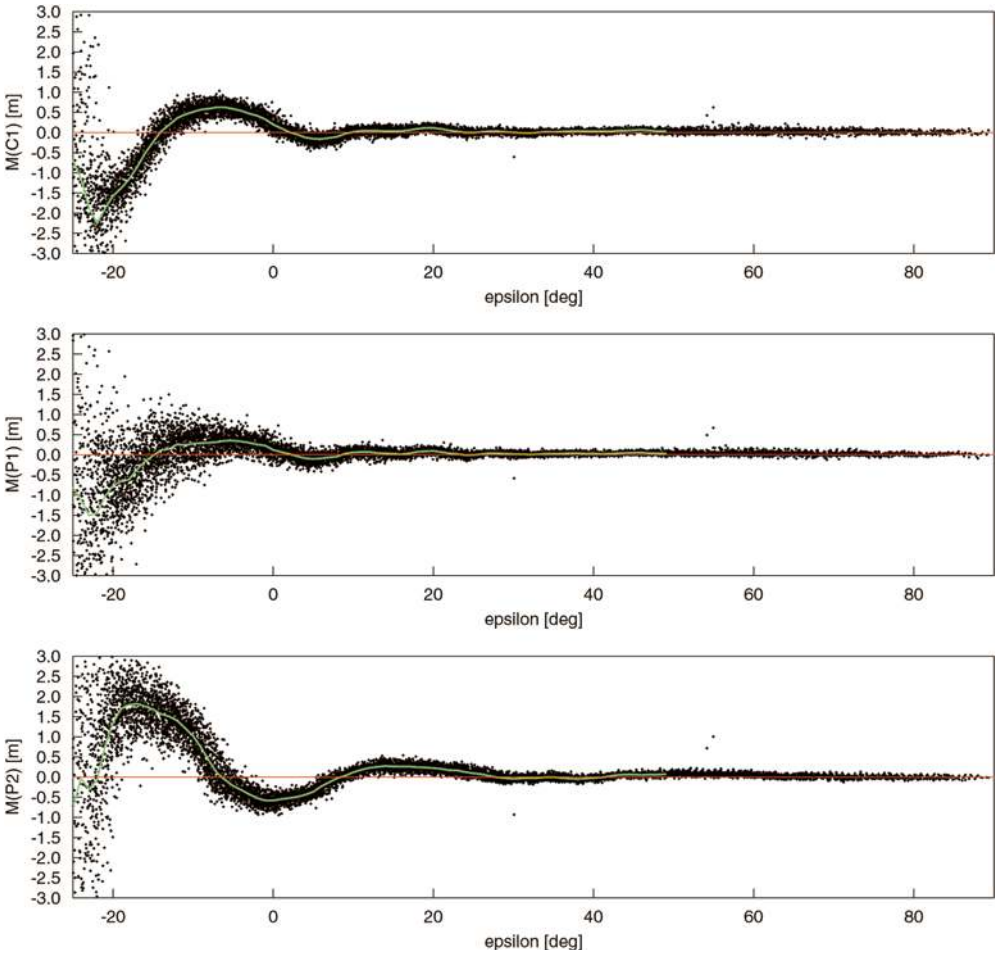

Fig. 6
Individual multipath measurements and elevation dependent mean value (*solid line*) for observations in the azimuth range α=180±10° (day 140–141/2001). For the selected observations, the elevation angle ϵ is roughly 27° smaller than the elevation E in the spacecraft frame

Table 3
Parameters of semi-empirical multipath model for CHAMP code measurements

Parameter		C/A	P_1	P_2
Reference amplitude	M_0	3.5 m	2.0 m	4.0 m
Central azimuth	α_0	200°	200°	200°
Reference elevation	ϵ_0	−27°	−27°	−27°
10dB scale height	$\Delta\epsilon_{10}$	25°	25°	35°
Wavelength	λ	0.1905 m	0.1905 m	0.2455 m
Constant path difference	$d_0 \bmod \lambda$	0.414 m	0.414 m	0.600 m
Baseline	b	0.36 m	0.36 m	0.45 m

types of code measurements. This may at least in part be justified by the assumption of different phase centers and antenna patterns for the L_1 and L_2 frequency, but is primarily motivated by a best fit of the observed multipath pattern. It may also be noted that the measured P_1 multipath error is roughly 40% smaller than the corresponding C/A-code error and no attempt has been made to explain this difference in terms of the applied correlation process.

Noise analysis

A good knowledge of the error distribution of code and carrier-phase measurements is of relevance for proper weighting and data editing in precise orbit determination applications. Other than in ground based signal simulator tests, a truth reference is not, however, available to determine the actual measurement errors of the CHAMP BlackJack receiver in orbit. Important information on the noise properties of the individual data types may nevertheless be obtained from a comparison of the independent code and carrier measurements in the C/A, P_1 and P_2 tracking channels.

Code noise

The analysis discussed above has shown that multipath errors only occur in the aft looking hemisphere. When confining oneself to observations in the forward part of the hemisphere the multipath terms disappear from Eq. (4), leaving only the noise related error of each code observable. In order to allow for a proper interpretation of the code noise, its standard deviation has been determined as a function of the carrier-to-noise-density ratio:

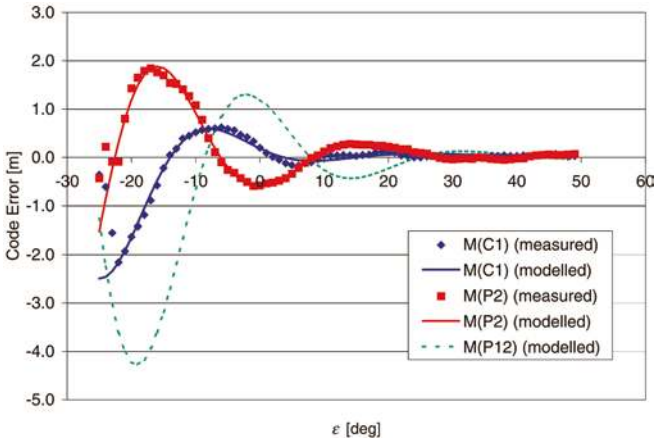

Fig. 7
Observed and modeled multipath errors within the azimuth range α=180±10°. The *dashed curve* denotes the predicted multipath error of the ionosphere-free linear combination $P_{12}=2.546\cdot P_1-1.546\cdot P_2$. For the selected observations the elevation angle ϵ is roughly 27° smaller than the elevation E in the spacecraft frame

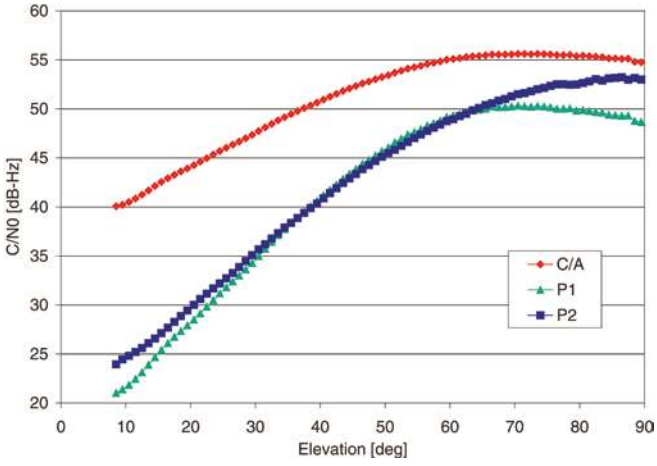

Fig. 8
Variation of carrier-to-noise-density ratio C/N_0 for C/A- and P-code measurements with elevation. Each point in the diagram represents the average C/N_0 value for observations collected in a ±0.5° wide elevation interval during days 245–248/2001

$$C/N_0 = 20 \cdot \log_{10}\left(\frac{SNR}{\sqrt{2}}\right) \quad (12)$$

(Young, personal communication). Here, SNR is the measured signal-to-noise ratio of the respective code observable as given in the RINEX data file (SA, S1, S2). The carrier-to-noise-density ratio (as well as the SNR value) is well correlated with elevation (Fig. 8) and varies between typical values of 40 dB-Hz at a lower threshold of 10° and 55 dB-Hz near the zenith for the C/A-code tracking channels. The corresponding P-code, in contrast, ranges from 20 to 53 dB-Hz as a result of the signal squaring required by the codeless tracking process (Young, personal communication).
In order to provide a good coverage of the lower C/N_0 range, multiple days have been analysed together. Results for days

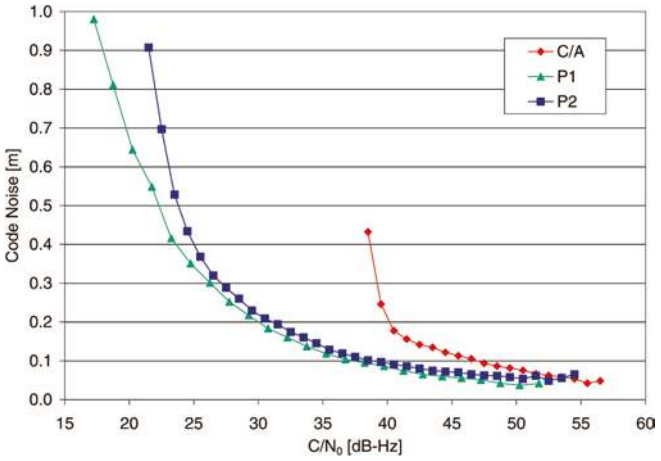

Fig. 9
Noise (1σ standard deviation) of C/A- and P-code measurements as a function of the carrier-to-noise-density. Each point in the diagram represents the average noise for observations within an interval of ±0.5 db-Hz (at high C/N_0) or ±0.75 db-Hz (at low C/N_0) during days 245–248/2001

245 to 248 of 2001 are given in Fig. 9, which shows that pseudorange noise of the carrier smoothed 10 s normal points varies between a minimum of 5 cm at high elevations and 0.5 m (C/A) or 1.0 m (P_1, P_2) at 10° elevation. The corresponding standard deviation of the unprocessed 1 s samples is roughly three times $(\sqrt{10})$ higher. No evidence of changes in the pseudorange noise distribution have been observed for selected data arcs between May 2001 (start of CHAMP data archive) and the end of 2002, but the code noise derived from the public Aug 2000 data set (day 220) is roughly twice as high. This may be attributed to the less effective normal point algorithm (quadratic pseudorange fit versus carrier smoothing) employed at this time.

Carrier noise

The BlackJack receiver provides two independent carrier-phase observables on the L_1 frequency (denoted as LA and L1), which are generated by the C/A-code and the P_1-code tracking channels. These observations are subject to the same ionospheric and multipath errors (cf. Eq. 1) and exhibit a maximum difference $|N_{L1}-N_{LA}|$ of one cycle count plus a line bias that is confined to less than a wavelength. Consequently, the difference $\rho_{L1}-\rho_{LA}$ is nominally constant throughout each pass, which can be used to assess the noise level of the carrier-phase measurements. In the absence of correlations, the standard deviation:

$$\sigma_{L1-LA} = \sqrt{\sigma_{L1}^2 + \sigma_{LA}^2} > \sigma_{L1} > \sigma_{LA} \quad (13)$$

thus provides an upper limit to the noise of the L1 and LA carrier-phase measurements. In view of squaring losses induced by the codeless tracking in the P_1 channel, it may further be assumed that the L1 standard deviation exceeds that of the LA measurements. Thus $\sigma_{L1\text{-}LA}$ provides a rough estimate of the L1 carrier-phase accuracy.
Key results of the carrier-phase noise analysis are presented in Figs. 10 and 11, which indicate notable

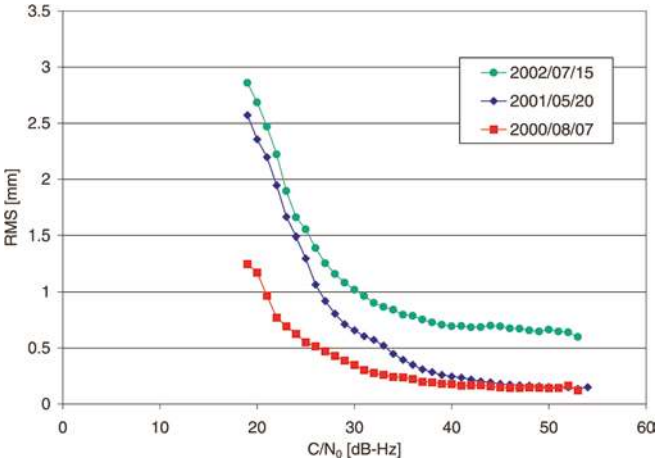

Fig. 10
Noise (1σ standard deviation) of L1-LA difference between L_1 carrier-phase measurements collected in C/A-code and P_1-code tracking channel as a function of P_1 carrier-to-noise-density ratio

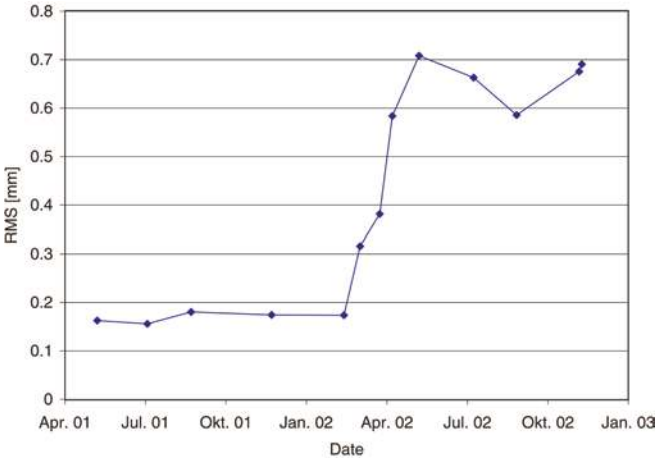

Fig. 11
Time history of L1-LA noise floor (1σ standard deviation at high C/N_0)

variations in the carrier tracking performance throughout the CHAMP mission. The lowest measurement noise level is achieved in the Aug 2000 data set, where the standard deviation of the L1−LA difference ranges from 0.15 mm at high elevations to 1 mm at low elevations. A roughly doubled noise level is encountered in carrier-phase measurements collected between May 2001 (start of CHAMP ISDC) and March 2002. While the noise floor at high C/N_0 remained at a constant level of about 0.2 mm during this period, it exhibits notable variations with peak values of 0.7 mm in the subsequent months. Even though the sudden change in the receiver performance is well correlated with the instance of the March 2002 software upload, no bandwidth changes have been performed at this time and it is unclear right now, whether other causes (thermal effects, oscillator behavior, etc.) contribute to the apparent degradation. Further observation of the carrier noise level is therefore suggested to collect additional information over the remaining mission lifetime.

Summary and conclusions

The in-orbit performance of the BlackJack dual-frequency GPS receiver onboard the CHAMP satellite has been analyzed using flight data collected between August 2000 and December 2002. Various software upgrades performed during this period have contributed to an improved data coverage and integrity, which is demonstrated for selected data arcs. At high elevations with good signal conditions representative noise levels of 5–10 cm for smoothed pseudoranges and 0.2–0.7 mm for carrier-phase measurements are achieved, which confirms the excellent overall quality of the geodetic grade receiver. Various types of data anomalies are discussed out of which the occasional 15 m code slips can be corrected using knowledge of the receiver internal sampling frequency. A cross-talk between the prime POD and occultation antenna strings has, furthermore, been demonstrated, which results in multipath-like pseudorange errors for observations collected in the rear hemisphere. A semi-empirical model is developed to describe the variation of these errors as a function of the line-of-sight vector in the spacecraft body frame and to allow a first-order correction of the affected measurements. It is expected that the results of the in-flight performance analysis facilitate the selection of adequate data editing and weighting strategies and contribute to a better understanding as well as further refinements of the BlackJack receiver hard- and software.

Acknowledgments The present study makes use of Blackjack GPS receiver measurements that have been made available for the CHAMP science team by GFZ, Potsdam. Precise reference orbits of the CHAMP satellite have kindly been provided by J. van den Ijssel, DEOS. Tom Meehan, JPL, and Ludwig Grunwaldt, GFZ, have taken the initiative for deactivating the occultation antenna string as part of a test campaign to demonstrate its impact on code multipath. Their support in this matter is highly appreciated. The authors would furthermore like to thank Larry Young, JPL, for his valuable comments and technical discussions during preparation of the manuscript.

References

Bertiger W, Bar-Sever Y, Desai S, Duncan C, Haines B, Kuang D, Lough M, Reichert A, Romans L, Srinivasan J, Webb F, Young L, Zumberge J (2000) Precise orbit determination for the shuttle topography mission using a new generation of GPS receiver; ION-GPS-2000. September 2000, Salt Lake City

Bertiger W, Bar-Sever Y, Dunn C, Haines B, Kruizinga G, Kuang D, Nandi S, Romans L, Watkins M, Wu S, Bettadpur S (2002) GRACE: Millimeters and microns in orbit; ION-GPS-2002, B5-5; Sept. 24-27, 2002, Portland Oregon

Braasch MS (1995) Multipath effects. In: Spilker J, Parkinson B, (eds) Global positioning system: theory and applications, vol I, chap. 14. American Institute of Aeronautics and Astronautics Inc, Washington

CHAMP (2000) CHAMP sample data set; ftp.gfz-potsdam.de/pub/champ/chftp1/public; In: CHAMP Newsletter No 2, Dec 8 (2000)

CHAMP (2001) Announcement of opportunity for CHAMP. CH-GFZ-AO-001, Issue 1.0, May 28, 2001, GeoForschungsZentrum Potsdam

Gurtner W, Estey L (2001) RINEX version 2.20 - Modifications to accommodate low earth orbiter data; IGS Mail 3281, April 12, 2001; ftp://ftp.unibe.ch/aiub/rinex/rnx_leo.txt

Haines B, Bertiger W, Desai S, Kuang D, Munson T, Reichert A, Young L, Willis P (2002) Initial orbit determination results for Jason-1: Towards a 1-cm Orbit. ION-GPS-2002, B5-4, Sept. 24-27, 2002, Portland, Oregon

Hofmann-Wellenhof B, Lichtenegger H, Collins J (eds) (1997) Global positioning system theory and applications,. 4th edn. Springer, Berlin Heidelberg New York

Köhler W (2001) CHAMP RINEX format observable extensions for CHAMP SST Data; http://op.gfz-potsdam.de/champ/docs_CHAMP/CH-RINEX-EXT.html, June 26, 2001

Kuang D, Bar-Sever Y, Bertiger W, Desai S, Haines B, Meehan T, Romans L (2001) Precise orbit determination for CHAMP using GPS data from BlackJack receiver. ION National Technical Meeting, Pap E1-5, January 22–24, Long Beach, California

Leva JL, de Haag MU, van Dyke K (1996) Performance of standalone GPS. chap. 7 In: Kaplan ED (ed) Understanding GPS principles and applications. Artech House

Lühr H, Grunwaldt L, Förste C (2001) CHAMP reference systems, transformations and standards. CH-GFZ-RS-002, Issue 2.1, Aug 30, 2001, GeoForschungsZentrum, Potsdam

Meehan TK (1997) SAC-C GPS TurboRogue space receiver - critical design review. SAC-C CDR TKM 09-16-97; JPL, Pasadena

Meehan TK (2001) History of CHAMP's operational changes and manoeuvres. CHAMP_rcvr.html, 16 Oct 2001, JPL, Pasa

Meehan TK, Thomas JB Jr, Young LE (2000) P-Code enhanced method for processing encrypted GPS signals without knowledge of the encryption code. US Patent 6 061 390, May 9, 2000

Melbourne WG (1985) The case for ranging in GPS-based geodetic systems; In: Goad C (ed) Proceedings of the 1st International Symposium on Precise positioning with the global positioning system. US Department of Commerce, Rockville, Maryland, pp 373–386

NASA (2001) BlackJack GPS receiver. NASA Tech Briefs NPO-20891, June 2001, http://www.nasatech.com/Briefs/June01/NPO20891.html

Reigber C, Bock R, Förste C., Grunwaldt L, Jakowski N, Lühr H, Schwintzer P, Tilgner C, (1996) CHAMP phase B—executive summary; Scientific technical report STR96/13, GeoForschungsZentrum Potsdam

Schutz BE (1998) Spaceborne laser altimetry: 2001 and beyond. In: Plag HP (ed) Book of extended abstracts WEGENER-98. Norwegian Mapping Authority, Honefoss, Norway

Sensor Systems (2002) GPS S67-1575 series data sheet. http://www.sensorantennas.com/pdf/1567-1575-14.pdf, Sensor Systems Inc, Chatsworth, California

Thomas JB (1995) Signal-processing theory for the TurboRogue receiver. JPL Publication 95-6, April 1, 1995

Van den Ijssel J, Visser P, Patiño Rodriguez E (2003) CHAMP precise orbit determination using GPS data. Adv Space Res (in press)

Williams J, Lightsey EG, Yoon SP, Schutz RE (2002) Testing of the ICESat BlackJack GPS receiver engineering model. ION-GPS-2002 Conference, 24–27 Sept. 2002, Portland, Oregon

Wübbena G (1985) Software developments for geodetic positioning with GPS using TI 4100 code and carrier measurements. In: Goad C (ed) Proceedings of the 1st International Symposium on Precise positioning with the global positioning system, US Department of Commerce, Rockville, Maryland, pp 403–412

Young LE, Meehan TK (1988) GPS multipath effect on code-using receiver. Presented at AGU, May 17, 1988, Baltimore, MD, USA